IEEE Access
Multidisciplinary | Rapid Review | Open Access Journal

Received February 5, 2021, accepted February 28, 2021, date of publication March 9, 2021, date of current version March 16, 2021.

Digital Object Identifier 10.1109/ACCESS.2021.3064638

A Feasible 3D Ultrasound Palmprint Recognition System for Secure Access Control Applications

ANTONIO IULA, (Senior Member, IEEE), AND MONICA MICUCCI
School of Engineering, University of Basilicata, 85100 Potenza, Italy
Corresponding author: Antonio Iula (antonio.iula@unibas.it)

ABSTRACT Biometric recognition systems based on 3D palmprint captured with optical technology have been widely investigated in the last decade; however, they can provide information about the external skin surface only. This limit can be overcome by Ultrasound, which allows gaining information on the depth of palm lines and can verify the liveness of the sample, making the recognition systems very hard to fake. In this work, a feasible palmprint recognition system based on 3D ultrasound images is proposed. Unlike previous wet setups, the coupling between probe and human is realized through a gel pad, which permits a comfortable and precise positioning of the hand by the user. Collected 3D images are processed to generate 2D palmprint images at various under-skin depths. 2D features are then extracted from these images, experimenting with different procedures, and are merged to define a 3D template that contains lines' depth information. Recognition performances were evaluated by performing verification and identification experiments on a home-made database composed of 423 samples from 55 volunteers. An EER rate of 0.36% and an identification accuracy of 100% are obtained. The suitability of the proposed system in secure access control applications is finally discussed.

INDEX TERMS Biometric, image processing, palmprint, ultrasound imaging.

I. INTRODUCTION

The increasing demand for biometric authentication systems has pushed scientific research to investigate and experiment with both new technologies to collect biometric characteristics and new techniques to extract features and to evaluate recognition accuracy.

Among the various biometric characteristics, palmprint is receiving a lot of attention by researchers due to its rich texture, which can be exploited both in law and forensic applications by capturing high-resolution images [1]–[4] and in a wide variety of access control systems by using low-resolution images [5]–[7]. For a long time, palmprint recognition was only based on features extracted from 2D optical images, which allow having quick and accurate systems [8], but can be easily forged [9]. In the last decade, however, a new modality for achieving 3D palmprint images, based on structured light imaging [9], [10], was set up and a wide research activity was dedicated to develop methods for extracting 3D features [11]–[16]. A possible limitation of these approaches could be because 3-D optical images provide information on the external skin surface only.

Palmprint has often been combined with other biometrics like palm vein pattern in multimodal systems [17]–[19], realizing a biometric fusion between the characteristics. This modality is frequently used because it offers several advantages, including an increase in recognition performances of the system.

Biometric recognition systems mainly collect images by using optical or infrared technology. Nevertheless, other approaches like Photoacoustics [20], [21] and Ultrasound [22] have been explored in recent years. The intrinsic capability of providing 3D information of the human body by Ultrasound can be profitably exploited in biometric systems for extracting richer features, increasing in this way recognition performances and allowing to extract features even if the skin is wet or abraded. Also, ultrasound images can automatically verify the liveness of a sample, for example by checking veins pulsing, which makes the systems hard to counterfeit. Wide research activity was dedicated to experimenting systems based on ultrasonic fingerprint, which is one of the most popular characteristics. Several kinds of such devices were proposed; in most cases fingerprint image was

The associate editor coordinating the review of this manuscript and approving it for publication was G R Sinha.

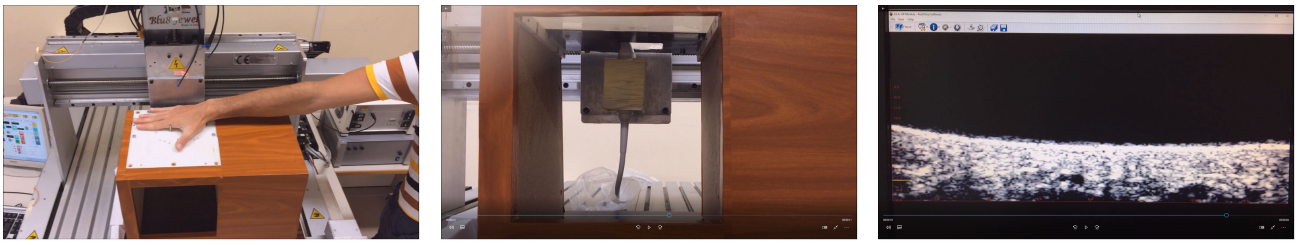

(a) (b) (c)

FIGURE 1. Set up for collecting 3D images: (a) the hand is positioned on a plastic plate where there is an open window filled with a gel pad and is aligned through some pegs, (b) the probe scan the palm from the upper side of the gel; (c) a collected b-mode image: liveness can be automatically detected by checking for vein pulsing.

obtained in pulse-echo modality with piezocomposite [23], cMUT [24]–[26] and pMUT [27]–[29] technologies. This last approach leads to a fingerprint scanner that was compatible with integration in smartphone devices [30], [31].

Palmprint is another biometric characteristic that can exploit ultrasound peculiarities. Palm area is much wider than fingerprint area and, therefore, a mechanical scan is needed, which make the system bulkier; on the other hand, features like principal lines and main secondary traits can be extracted from low-resolution images and hence with lower frequency probes, making the technological problem less challenging. The authors' research group experimented with some possible set up for collecting 3D ultrasound images of palmprint [32], [33]. 3D features were consequently extracted with methods based on palm curvature analysis [34], following a similar approach as the one used with optical images [9]. To fully exploit 3D information present in the ultrasound image, another feature extraction method, based on the analysis of principal lines under-skin depth, was proposed and experimentally evaluated [35], demonstrating excellent recognition results. In these works, image acquisition was carried out by submerging in a water tank both probe and human hand, for water guarantees a very good acoustic coupling. However, such wet acquisition modality could be hardly used in applications because user acceptance is expected to be very low due to the necessity to immerse the hand in a tank of water. Another drawback is the uncomfortable position of the hand when it is immersed, which led to many bad samples because the user had difficulty holding the correct position during the acquisition.

To overcome these problems, a new feasible setup is assembled providing that the user may comfortably place the hand on a base and a commercial gel pad, usually used in pediatric diagnostic applications, plays as coupling medium. First experiments [36] demonstrated that the features extraction procedure used in the wet system didn't work adequately with the new images. Consequently, other procedures for 2D features extraction [37]–[39] and a first attempt to generate a 3D template [40] were experimented and preliminary tested on small databases.

In this work, a complete 3D Ultrasound Palmprint recognition system is proposed and experimentally evaluated through a much more consistent home-made database. Recognition performances achieved with four different 2D features extraction methods are compared and the one that provided more accurate results is selected for 3D analyses. A 3D template is then generated by opportunely combining 2D templates excerpted at several depths inside the skin. Verification and identification experiments are finally carried out to verify the recognition capabilities of the system.

From now on, section II illustrates the set up used for collecting 3D images; section III presents feature extraction procedures for generating 2D and 3D templates; section IV reports verification and identification experiments carried out to evaluate the systems, and section V contains the conclusion and a discussion on the potentiality of the proposed system.

II. 3D IMAGE ACQUISITION

3D ultrasound imaging is intensively used in a large number of medical diagnostic applications [41]–[44] because of its capability to provide an accurate description of human organs with no ionizing radiations and lower cost than computer tomography and magnetic resonance. In this work, 3D images of a portion of the human hand were collected by using a high frequency commercial linear array (LA435 by Esaote S.p.A., Italy), which is moved by a numerical pantograph to scan the region of interest [39]. This approach guarantees a higher resolution and a larger field of view if compared to a 3D ultrasound probe [45]. The array, which has a central frequency of 12 MHz and an aperture of almost 40 mm, is controlled by the ULA-OP ultrasound scanner [46]. A 20 mm thick gel pad was employed as coupling medium; this material ensures an acoustic coupling slightly worse than water [35], yet this solution allows to obtain a comfortable and precise positioning of the hand and, not less important, is expected to be much more acceptable by users. Figure 1 shows some frames of a movie that describes the set up and an example of image capturing (see also attached video). During the acquisition, the liveness of the sample can be automatically detected by verifying the pulsing of veins. It is to highlight that the whole acquisition system, including the electronics, could be easily contained in a compact box, even smaller than the one used for experiments, by substituting the bulky pantograph with a simple stepper motor.

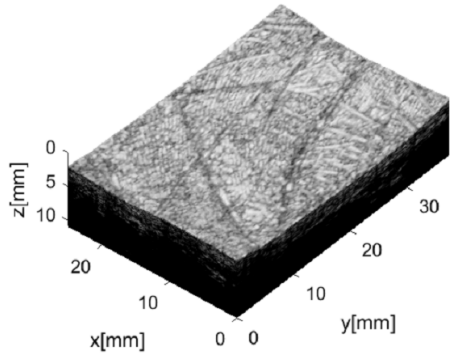

FIGURE 2. Example of 3D rendering of a palmprint ultrasound image.

During the motion over the region of interest, which is 50 mm long, 250 B-mode images like the one shown in Figure 1c are collected and stored. The resulting volumetric image is cropped to eliminate border values reducing the useful volume to $25 \times 38 \times 11$ mm^3. After an interpolation, carried out to obtain a pixel spacing of 46.2 μm along the three directions, the volume remains represented by a $542 \times 814 \times 238$ matrix of voxels, where voxel's brightness has a grayscale dynamic of 8-bit. Figure 2 shows a 3D image of the palm obtained with a global thresholding operation [47], [48], which eliminates black voxels corresponding to the gel cushion. This volume contains at least two kinds of 3D information that can be used for recognition purposes: the 3D profile of palm curvature [34], which may be also extracted from optical images collected with structured light scanners [9], [12]; and the depth of principal lines and main traits, which is contained in under-skin layers [35] and, therefore, cannot be achieved with optical images.

A recognition procedure based on this last modality is implemented by excerpting several 2D images at various depths from the volume shown in Figure 2. The first 2D fingerprint image is obtained by projecting the 3D profile $P_1(x, y, z)$ of the external surface of the palm on the xy plane. Then, a 3D profile $P_2(x, y, z)$, parallel to $P_1(x, y, z)$ but translated of 46.2 μm, i.e. one pixel, along z inside the skin, is projected on the xy plane to achieve the second 2D palmprint image. Similarly, other 2D images are extracted at increasing under-skin depths until information on lines and traits is no more distinguishable. Figure 3 shows the 7 shallowest 2D images extracted with the above-reported procedure. We can observe that, as the depth increase, some traits become less evident while some others remain recognizable. It can also be seen that the seventh image is much darker than the previous ones. Deeper images are increasingly darker and, therefore, they are not used for features extraction.

III. FEATURE EXTRACTION

To achieve a template that contains information of principal lines' depth, four procedures for extracting a feature from 2D images are evaluated. Then, the best of them is applied to all images shown in Fig. 3 to obtained n 2D templates, which are opportunely combined to generate a 3D template.

A. 2D FEATURE EXTRACTION

A wide variety of methods to extract features from a 2D image of palmprint can be found in the literature [49], [50]. In [35], a classical line detection procedure was used for ultrasound images collected by using water as coupling medium, obtaining good results. However, as shown in [36], that procedure provided unsatisfactory results with images acquired by using gel as coupling medium.

To improve the accuracy of 2D features, several procedures were experimented with and compared in this work. All these methods perform, at a certain stage and in different ways, a filtering operation aimed to reduce speckle noise, generated by the interference between transmitting and receiving waves, which inherently affects ultrasound images [51]. Speckle noise is a multiplicative noise with a granular pattern that deteriorates both resolution and contrast of the image; it depends on several parameters, including the kind of probe, its distance from the target and the operating frequency. One of the most popular approaches to reduce speckle noise is based on the use of spatial domain methods [52]–[55]. In the present work, two of these techniques are evaluated: Frost [56], [57], which is, basically, an adaptive filter that uses exponentially weighting factors depending on the variance; and Speckle Reducing Anisotropic Diffusion (SRAD) [58], [59], which is a non-linear filter able to reduce multiplicative noise.

Main operations of the first procedure [37], called here "Method A", are summarized below:

- Frost filter;
- Normalization;
- Bottom-hat;
- Morphological operations;
- Resize.

After the Frost filter stage, a normalization of gray levels was performed, to minimize differences between max and min values of the input image; then, a bottom-hat transformation [60], [61] highlights the palmprint lines that have to be detected. The image is then binarized by choosing a suitable threshold and some classical morphological operations (closing, thinning and pruning) are performed. Finally, the image is resized to a dimension of 107×160 pixels, to speed up subsequent matching operations.

"Method B", instead, experiments a SRAD filter to reduce speckle noise and a Derivative of Gaussian (DoG) filter [62], [63], which is a bandpass filter able to eliminate spatial frequencies that are too far from the center of the band; in this way, edges are expected to be enhanced. In this method, the resize operation is performed at the beginning to diminish also the processing time needed to obtain the template. Also, in this case, binarization is performed by using a fixed threshold. Similar morphological operations as the previous method were finally carried out. The main steps of "Method B" are resumed as follow:

- Resize;
- SRAD filter;

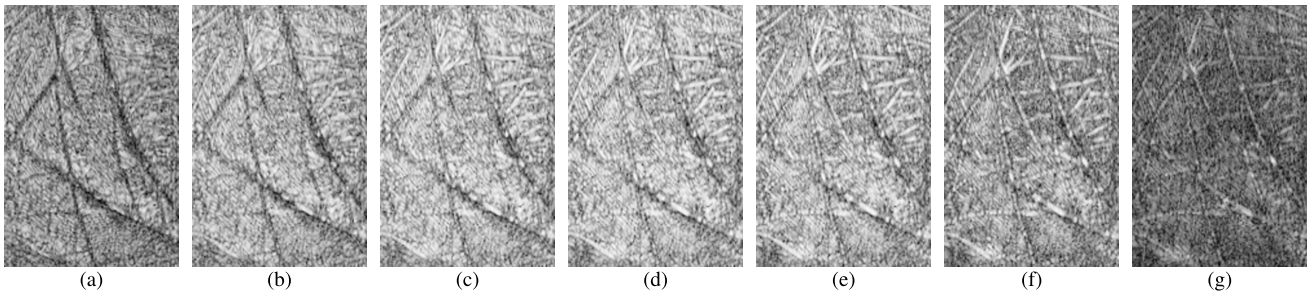

FIGURE 3. 2D palmprints extracted at increasing under skin depths with step 46.2 μm: (a) is the superficial one and (g) corresponds to a depth of about 323 μm.

- DoG filter;
- Morphological operations.

"Method *C*" [40] uses SRAD filter and bottom-hat; this last transformation is performed along four directions and the resulting images are summed through an OR operation. After a contrast adjustment, the image is binarized with an adaptive threshold, determined by the analysis of the histogram reporting the number of pixels for each level gray. Other morphological operations were performed before the final resize. Here below the sequence of operations:

- SRAD filter;
- Bottom hat along four directions: 0°, 45°, 90°, 135°;
- Logical sum;
- Contrast adjustment;
- Morphological operations;
- Resize.

The last procedure, indicate here as "Method *D*", was described in detail in [39]. It was based on an approach proposed in [64] and consists of a higher number of steps than the previous ones with the aim to achieve more accurate results:

- Contrast adjustment;
- Resize;
- Frost filter;
- Contrast adjustment;
- Normalization;
- Median filter, only along 0°;
- Mean filters along four directions: 0°, 45°, 90°, 135°;
- Bottom hat along four directions: 0°, 45°, 90°, 135°;
- Logical sum;
- Morphological operations.

In this case, after a first contrast adjustment, the image is scaled down and deformed to a square matrix of 128 × 128 pixels to perform in a more effective way filter and transformation along diagonal directions. The image obtained is filtered using Frost filter and then another contrast adjustment is performed. The next operations are the normalization and the clonation to obtain four copies of the image to be processed along four different directions (0°, 45°, 90°, 135°). A median filter is applied only to image along direction 0°,in order to reduce salt and pepper noise, and then mean filters and bottom-hat operations are applied along the four directions. Obtained images are summed through logical OR.

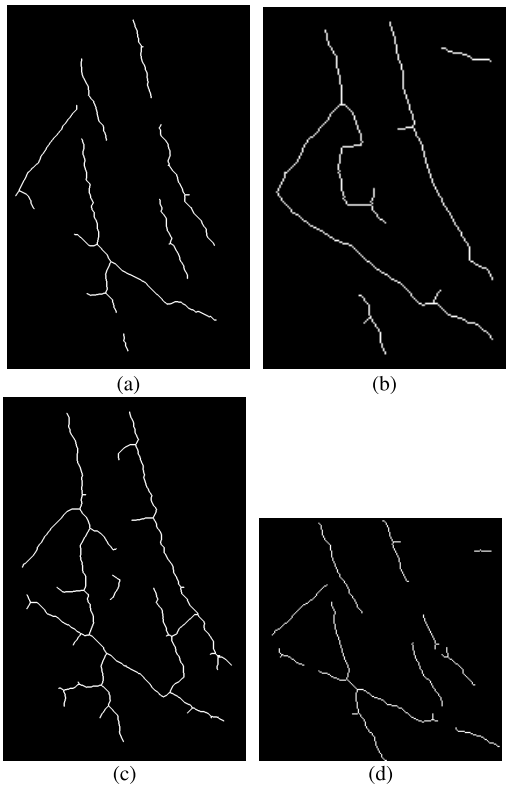

FIGURE 4. Templates obtained with the various procedures from the 2D image of Figure 3a: (a) "Method *A*", (b) "Method *B*", (c) "Method *C*", (d) "Method *D*".

Finally, binarization with a fixed threshold and morphological operations are performed.

Figure 4 shows the templates generated with each of the four methods from the image of Figure 3a.

Each of these procedures was evaluated with preliminary tests carried out on a small number of samples. In this work, they are compared by using the same database, which contains a much greater number of samples than those previously employed.

B. 3D TEMPLATE GENERATION

The procedure used to generate a 3D template able to account for palmprint lines' depth receives as input the 2D templates extracted from the 2D palmprint images of Figure 3 with one of the procedures described in the previous section. Figure 5

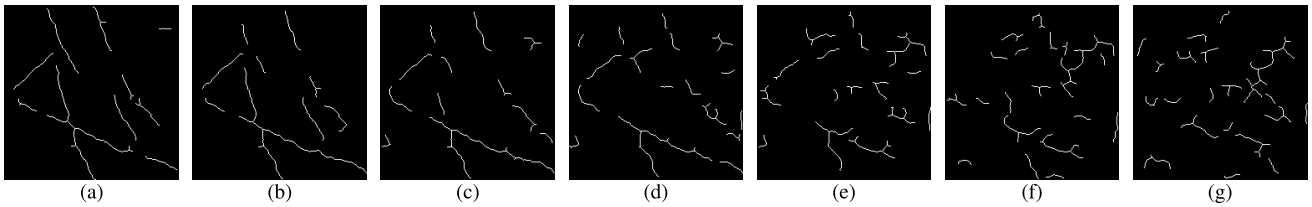

FIGURE 5. The 7 templates extracted with "Method *D*" from the corresponding 2D images of Figure 3.

shows the results obtained by using ''Method *D*''. As can be seen, by increasing the under skin depth, the template contains less and less information on principal lines and, moreover, an increasing number of secondary traits, not present in the first template, appears.

To generate the 3D template, it is assumed that the 2D template extracted from the shallowest image (Figure 5a) contains the maximum information and therefore only the traits present in this template are those on which the depth is evaluated. As a consequence, white pixels of deeper templates, in different positions than those of the first template, have to be eliminated.

The 3D template is then defined as a 3D matrix $A(i, j, k)$, where the $i \times j$ dimension is the same as that of the 2D template and the k dimension is n, i.e., the number of 2D templates: in this work n=7. $A(i, j, 1)$ is obtained by performing a DILATE operation on the shallowest template. Then, $A(i, j, k)$ is achieved by performing a logical AND operation between corresponding pixels of $A(i, j, k - 1)$ and the k shallowest template; the result is dilated and stored.

The AND operation ensures that the $A(i, j, k)$ will not present new traits concerning $A(i, j, k - 1)$; therefore, it may be considered as a filter for spurious traits that may appear in deeper images.

The DILATE operation is introduced to consider that the depth of a palmprint line may be not perpendicular to the $x-y$ plane and, therefore, the same trait in a template extracted at a given depth may be slightly translated concerning the shallower template or to the deeper one. The dimension β of the structured element used for the dilation is a parameter that has to be optimized because if it is too large, spurious traits could be included, while if it is too small, traits belonging to a principal line but not exactly perpendicular to the $x - y$ plane could be eliminated.

Figure 6a shows a representation in the colour scale of the 3D template generated by setting the dimension of the DILATE operator to 4; this value was determined in a heuristic way. The 2D image corresponding to the shallowest 2D Palmprint (Figure 3a) after the resize operation is reported in Figure 6b for comparison. Each pixel value ranges from 0 (blue), when a trait is never detected in any 2D template, to 6 (red), when it is detected in all the 2D templates. Further examples of 3D templates with the corresponding 2D grayscale images are reported in Figure 7: same user as Figure 6 but collected at a different time in Figure 7a, other users in Figures 7b and 7c.

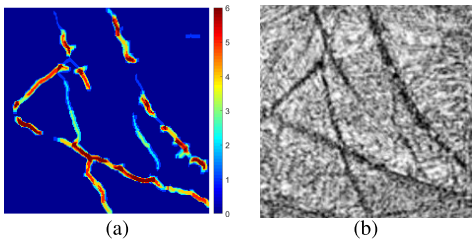

FIGURE 6. (a) 3D template obtained from 2D templates of Figure 5; (b) the shallower 2D image (see Figure 3a) after resizing.

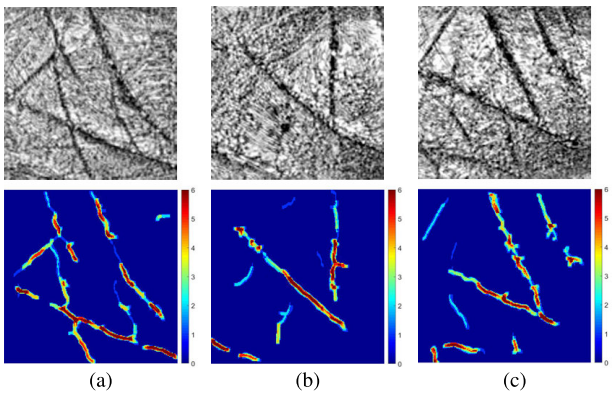

FIGURE 7. Three more examples of 2D images with the corresponding templates: (a) is captured from the same user as Figure 6 but at a different time; (b) and (c) belong to two different users.

IV. RECOGNITION RESULTS

An evaluation of the recognition capability of the proposed system is carried out by performing both verification and identification experiments on a home-made database composed of 423 samples collected from 55 different adult individuals of both sexes with the experimental setup described in Figure 1.

A. VERIFICATION EXPERIMENTS

Verification is a recognition modality that has the aim to authenticate a person based on the claimed identity. A verification system is therefore a one to one system that performs a match between a query template, extracted from a sample released by a user, with the stored reference template, which was been previously generated from another sample of the declared individual.

In this work, for both 2D and 3D cases, verification experiments were executed by comparing each template with all the others in the database. This approach allows having a

higher number of scores than the classical reference-query one, proving more reliable results.

1) COMPARISON AMONG 2D METHODS

The method adopted to calculate the matching score between two 2D templates is based on a classic pixel-to-area comparison [9], [49], which basically performs a logical AND operation between corresponding pixels of the two images and then normalizes the result to the arithmetic mean of the total number of white pixels present in the comparing images:

$$S_{2D}(R, Q) = \frac{2}{M_R + M_Q} \sum_{i=1}^{n} \sum_{j=1}^{n} R(i, j) \oplus Q(i, j) \qquad (1)$$

where R and Q are the reference and query binary images, respectively, M_R and M_Q are the sum of white pixels in R and Q, respectively, and $n \times n$ is template dimension.

A possible incorrect alignment of the hand was taken into account by performing the match several times while translating and rotating the query template of a small quantity. The highest score is the one used in statistic analysis [9].

If the two matched templates belong to the same user, the score is registered as a genuine match while, if they belong to different users, the score is registered as an impostor match. The user is authenticated if the matching score exceeds a predefined threshold, which depends on the application. If an impostor score results higher than the threshold, a False Acceptance error is committed; on the other hand, if a genuine score is lower than the threshold, a False Rejection error occurs. For each value of the threshold, False Acceptance Rate (FAR) and False Rejection Rate (FRR) can be computed as the ratio of the number of false acceptance and rejection and the total scores, respectively. It is intuitive than by increasing the threshold from 0 to 1, FAR grows from 0 to 100% while FRR decreases from 100% to 0. There is a threshold value for which FAR=FRR: the corresponding error rate is called Equal Error Rate (EER). This parameter is often used for evaluating and comparing different biometric recognition systems.

Recognition performances of biometric systems are usually compared through Detection Error Tradeoff (DET) curves, which plot FAR vs FRR. Figure 8 shows DET curves for the four 2D features extraction procedures described in section III. The closer the curve to the axes, the better the recognition performances of the system. As can be seen "Method D" is clearly the best. In this plot, the EER value of each procedure can be obtained by calculating the intersection of the curves with the first bisector. The numerical values of the EER have reported in Table 1 together with two other parameters that allow comparing the various methods in term of computational cost: Feature Extraction Time (FET) and Matching Time (MT). As can be seen, "Method D" is the second fastest after "Method B", which however exhibits a much higher EER. The hardware used for simulations is an Intel(R) Core(TM) i9-9900 processor @3.10 GHz with 32GB RAM.

TABLE 1. EER values, features extraction time (FEA) and matching time (MT) for the four 2D methods.

	Method A	Method B	Method C	Method D
EER (%)	4.05	5.11	1.95	0.52
FEA (s)	7.3	0.33	0.8	0.74
MT (s)	0.6	0.56	1.8	0.8

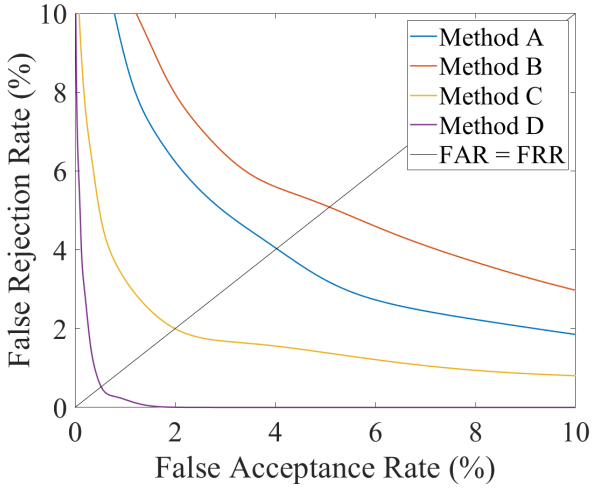

FIGURE 8. DET curves for the four 2D features extraction methods. The EER is given by the intersection of the curves with the first bisector (FAR=FRR).

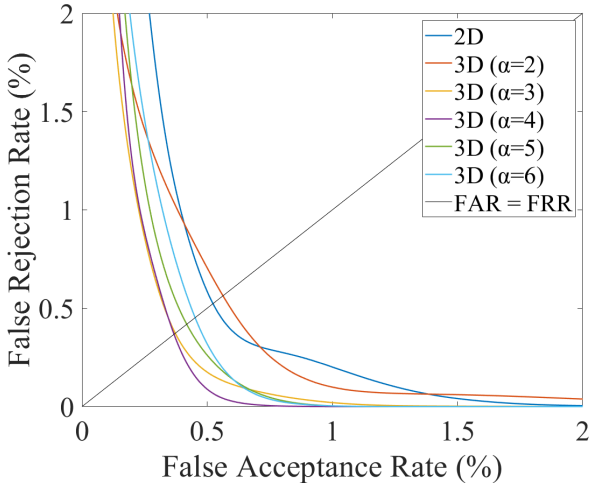

FIGURE 9. DET curves obtained with the 3D method for various values of α; the best result obtained with the 2D method is reported for comparison.

2) 3D METHOD

As "Method D" clearly provided the best 2D recognition results, verification experiments were carried out by using only 3D templates generated with this method. The matching formula (1) for 3D comparisons has been modified as follow:

$$S_{3D}(R, Q) = \frac{2}{M_R + M_Q} \sum_{i=1}^{n} \sum_{j=1}^{n} R(i, j, 1) \oplus Q(i, j, 1) \oplus |O_R(i, j) - O_Q(i, j)| < \alpha \qquad (2)$$

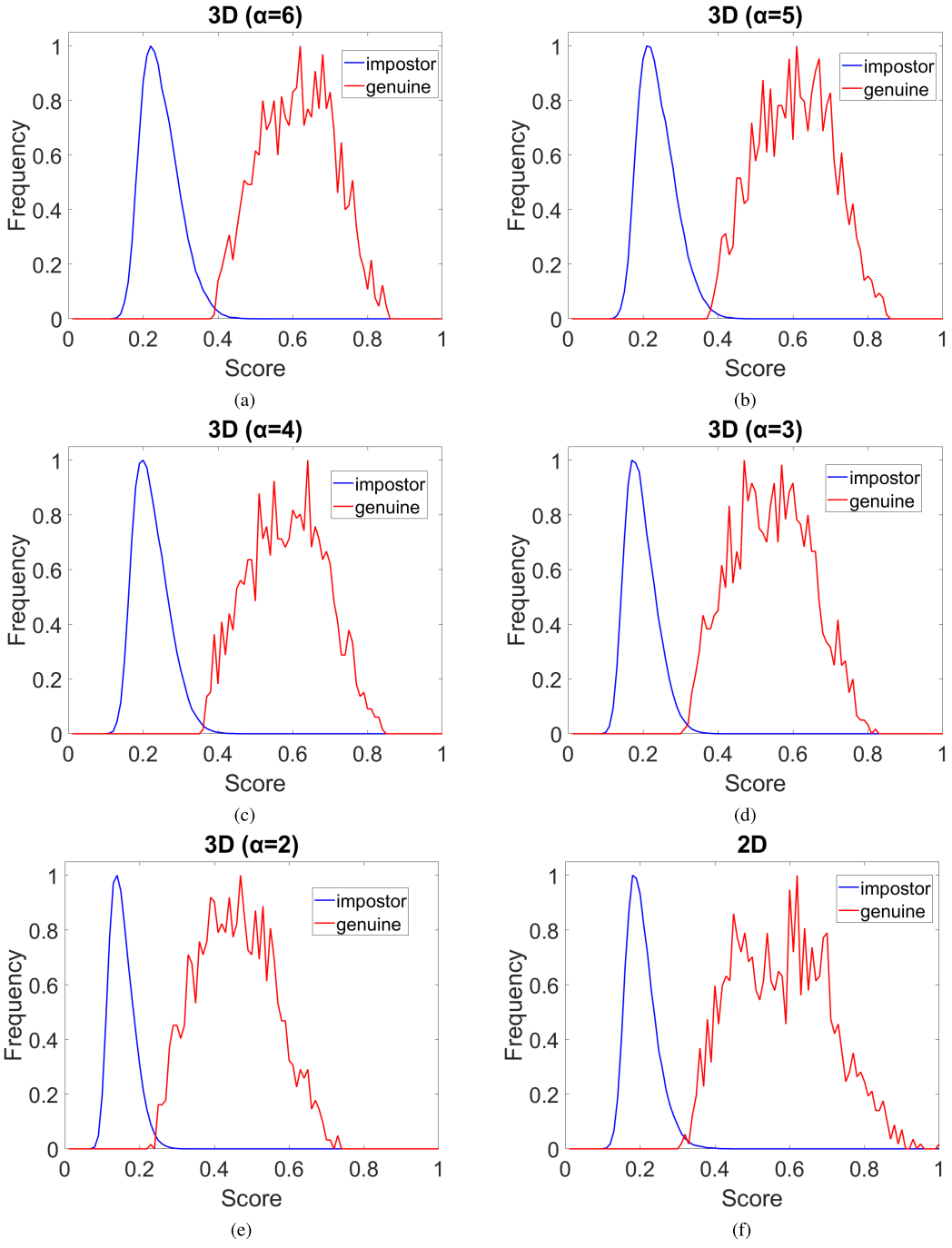

FIGURE 10. Impostor and genuine distributions obtained with the 3D method for α ranging from 6 (a) down to 2 (e) and with the 2D method (f).

where $R(i, j, 1)$ and $Q(i, j, 1)$ are the 3D reference and query templates, respectively, at level 1, α is an integer with values ranging from 0 to the number of levels N in the 3D template and $O_R(i, j)$ and $O_Q(i, j)$ are the occurrences of value "1" in $R(i, j, k)$ and $Q(i, j, k)$. The condition $|O_R(i, j) - O_Q(i, j)| < \alpha$ guarantees that the result of the comparison for each pixel is "1" only if the difference of occurrences between R and Q is lower than α. The lower α the higher the similarity requested for the two comparing templates. Similar to the 2D cases, various comparisons were made by performing small rotations and translations of the query template to account for incorrect positioning during the acquisition.

The times for generating a 3D template and for performing a 3D matching were 0.26 s and 2 s, respectively.

Figure 9 shows DET curves obtained for several values of α. In the plot, the DET curve obtained for the best 2D case, i.e., by using "Method D", is also plotted for comparison. As can be seen, the use of a 3D template allows to improve 2D recognition performances almost for any value of α, best results being achieved for α=3 and α=4.

TABLE 2. Mean and standard deviation of impostor and genuine distributions and EER calculated for the various recognition methods.

	Mean		Standard Deviation		EER (%)
	Impostor	Genuine	Impostor	Genuine	
2D	0.205	0.579	0.040	0.129	0.52
3D (α=2)	0.154	0.456	0.032	0.102	0.56
3D (α=3)	0.196	0.542	0.041	0.105	0.36
3D (α=4)	0.222	0.584	0.046	0.103	0.36
3D (α=5)	0.239	0.604	0.049	0.101	0.41
3D (α=6)	0.247	0.611	0.05	0.099	0.45

TABLE 3. Mean, standard deviation and occurrences of NSD < 0.2 for the distributions of Figure 12.

	Mean	Standard Deviation	NSD < 0.2
2D	0.297	0.126	102
3D α =3	0.286	0.108	78
3D α =4	0.272	0.101	84

To further deepen the influence of α on the recognition performances of the system, a statistical analysis on impostor and genuine distributions was carried out. Figure 10 shows the distributions of genuine and impostor scores obtained with the 3D method, for various values of α, and with the best 2D method. In the plots, recognition error quantity is proportional to the area generated by the intersection of the impostor and genuine distributions. For each distribution, mean and standard deviation value are computed and results are shown in Table 2 together with the ERR values. As can be seen, by increasing α, a growth of the mean value is observed for both impostor and genuine score distributions and for impostor standard deviation. The standard deviation of genuine, instead, is almost constant for any α. Results obtained with 2D templates show that impostor and genuine's mean and impostor standard deviation have values intermediate to those obtained with α=3 and α=4 in the 3D case, while 2D genuine standard deviation is sensibly higher than all 3D one's. Hence, it appears that the improvement of recognition performances obtained with the 3D method is to be attributed to this last behaviour.

To verify the optimal value of the dimension β of the structuring element for the dilate operation in 3D template generation, several simulations were performed. Figure 11 shows the DET curves obtained for various values of β when α=4. As can be seen, best performances are obtained for β=4. This result was confirmed for other values of α as well.

If compared with the wet system experimented in [35], the present one exhibits only slightly worse recognition performances in verification modality (EER 36% vs 21%), while it shows an improvement concerning results obtained in [34], where a 3D feature extraction based on curvature analysis was adopted. Other comparisons could be done with performances of 3D palmprint recognition system that uses optical technologies for collecting the images reported in [16] (Table 3) or in [35] (Table 2). In general, a direct comparison should require similar experimental conditions, databases etc.; anyway, it can be asserted that the recognition rate of the proposed system is more than satisfactory and suitable for practical applications.

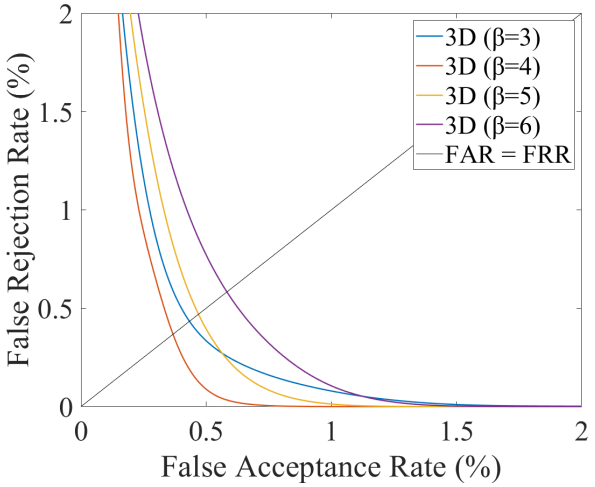

FIGURE 11. DET curves obtained with α=4 for various values of β.

B. IDENTIFICATION EXPERIMENTS

Different from verification, identification modality tries to establish the identity of an unknown person. The system in this case compares a test template with all templates contained in a database: the highest score determines the identity if it exceeds a predefined threshold; otherwise, the person is considered as not present in the database. Identification experiments were performed by comparing each 3D template with all the remaining ones. Following this approach, results are scheduled in 423 tables: each table contains 422 scores, ordered from highest to lowest, with m genuine and n impostor scores. Matching obtained by setting both α=3 and α=4 were evaluated; a similar analysis was carried out by using 2D templates as well. In any case, all the m genuine scores ranked in first places, meaning that the identification rate is 100%. It is to point out that identification experiments carried out in this way result more stringent concerning the classical methods, which compare an example with only one template for each member of the population. To further test the robustness of the identification procedure, the distance between the lowest genuine score and best impostor score, which is the worse case, was calculated for all experiments. Figure 12 shows the distribution of such values, normalized to the lowest genuine score, obtained by setting α=3 (a) and α=4 (b). The same distribution achieved by matching 2D templates is shown in Figure 12c for comparison. For each of these distributions mean and standard deviation were computed and results are reported in Table 3. As can be seen, on one hand, 3D distributions exhibit a lower mean value than the 2D one, which would be not desirable, but on the other hand, they present a lower standard deviation, which instead is a merit because it ensures that a lower number of score differences is close to 0. To better investigate this behaviour, a further parameter is tabulated: the occurrences of Normalized Score Differences (NSD) that assume a value

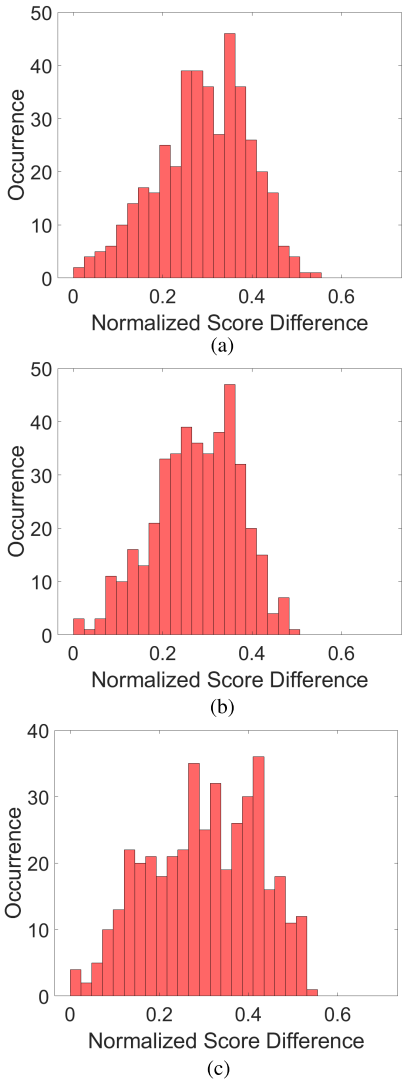

FIGURE 12. Distribution of the distance of the highest impostor score from the lowest genuine one, normalized to the genuine: (a) 3D (α=3), (b) 3D (α=4) and (c) 2D.

less than 0.2 (NSD < 0.2). This value is sensibly higher in the 2D distribution, demonstrating that the 3D method is much more robust than the 2D one.

V. DISCUSSION

As shown in the previous section, the proposed system provided quite similar recognition results as the wet one presented in [35] but, due to the natural position of the hand, the number of discarded acquisitions was dramatically reduced. In addition, it proved much more acceptable by users, which is a very important factor in practical biometric systems. The achieved recognition rate was anyway comparable with that of the majority of optical unimodal palmprint systems.

The proposed approach has the further merit of being able to automatically detect the liveness of the sample by checking vein pulsing during image acquisition, which makes it very difficult to spoof. Furthermore, the same volumetric image can be exploited for extracting other 3-D palmprint features through curvature methods [34] as well as other features than palmprint like inner hand geometry [65], hand geometry [66], [67] and vein pattern [68], [69], implementing in this way a hand-based multimodal system, which is expected to improve the overall performances of the system.

The 3-D technique also benefits from other advantages of Ultrasound, including not being sensitive to many kinds of surface contamination, humidity and environment light or temperature.

Despite the achieved results, the acquisition system could be still improved by realizing an ergonomic pad, made of polydimethylsiloxane (PDMS) [26] or similar composite, to allow an even more precise and comfortable position of the hand and by experimenting with improved beamforming techniques, which are currently under study, to enhance image quality and repeatability. Furthermore, advanced techniques exploited in biometric recognition, like machine learning techniques [70]–[73], could be profitable experimented on ultrasound images as well. To this end, a new and more consistent database should be established to provide a more reliable evaluation of the system.

A main drawback of the systems is its relatively high total cost, which however could be sensibly contained by using compact and cheap ultrasound scanners that recently appeared on the market [74] that use probes based on the emerging CMUT technology [75], [76].

VI. CONCLUSION

In this work, a feasible palmprint recognition system based on 3D ultrasound imaging is proposed and experimentally evaluated. A gel pad was employed to couple human hand and probe, providing a precise and comfortable positioning for the user. A 3D template that contains information on the depth of principal lines and main wrinkles was generated by opportunely combining 2D templates extracted from images collected at several under-skin depths. The system was evaluated through verification and identification experiments carried out on a preliminary home-made database, which demonstrate that recognition accuracy is more than satisfactory and suitable for practical applications, especially in high secure access control field.

ACKNOWLEDGMENT

The authors thank Dott. Donatella Nardiello for his help in collecting experimental data.

REFERENCES

[1] J. Dai and J. Zhou, "Multifeature-based high-resolution palmprint recognition," *IEEE Trans. Pattern Anal. Mach. Intell.*, vol. 33, no. 5, pp. 945–957, May 2011.
[2] R. Cappelli, M. Ferrara, and D. Maio, "A fast and accurate palmprint recognition system based on minutiae," *IEEE Trans. Syst., Man, Cybern. B. Cybern.*, vol. 42, no. 3, pp. 956–962, Jun. 2012.
[3] R. Wang, D. Ramos, R. Veldhuis, J. Fierrez, L. Spreeuwers, and H. Xu, "Regional fusion for high-resolution palmprint recognition using spectral minutiae representation," *IET Biometrics*, vol. 3, no. 2, pp. 94–100, Jun. 2014.

[4] S. Chen, Z. Guo, J. Feng, and J. Zhou, "An improved contact-based high-resolution palmprint image acquisition system," *IEEE Trans. Instrum. Meas.*, vol. 69, no. 9, pp. 6816–6827, Sep. 2020.

[5] D.-S. Huang, W. Jia, and D. Zhang, "Palmprint verification based on principal lines," *Pattern Recognit.*, vol. 41, no. 4, pp. 1316–1328, Apr. 2008.

[6] L. Zhang, H. Li, and J. Niu, "Fragile bits in palmprint recognition," *IEEE Signal Process. Lett.*, vol. 19, no. 10, pp. 663–666, Oct. 2012.

[7] D. Palma, P. L. Montessoro, G. Giordano, and F. Blanchini, "Biometric palmprint verification: A dynamical system approach," *IEEE Trans. Syst., Man, Cybern. Syst.*, vol. 49, no. 12, pp. 2676–2687, Dec. 2019.

[8] D. Zhong, X. Du, and K. Zhong, "Decade progress of palmprint recognition: A brief survey," *Neurocomputing*, vol. 328, pp. 16–28, Feb. 2019.

[9] D. Zhang, G. Lu, W. Li, L. Zhang, and N. Luo, "Palmprint recognition using 3-D information," *IEEE Trans. Syst., Man, Cybern. C, Appl. Rev.*, vol. 39, no. 5, pp. 505–519, Sep. 2009.

[10] W. Li, D. Zhang, G. Lu, and N. Luo, "A novel 3-D palmprint acquisition system," *IEEE Trans. Syst., Man, Cybern. A, Syst. Humans*, vol. 42, no. 2, pp. 443–452, Mar. 2012.

[11] J. Ni, J. Luo, and W. Liu, "3D palmprint recognition using Dempster-Shafer fusion theory," *J. Sensors*, vol. 2015, pp. 1–7, Feb. 2015.

[12] X. Bai, N. Gao, Z. Zhang, and D. Zhang, "3D palmprint identification combining blocked ST and PCA," *Pattern Recognit. Lett.*, vol. 100, pp. 89–95, Dec. 2017.

[13] B. Yang, X. Xiang, D. Xu, X. Wang, and X. Yang, "3D palmprint recognition using shape index representation and fragile bits," *Multimedia Tools Appl.*, vol. 76, no. 14, pp. 15357–15375, 2017.

[14] Ö. Bingöl and M. Ekinci, "Stereo-based palmprint recognition in various 3D postures," *Expert Syst. Appl.*, vol. 78, pp. 74–88, Jul. 2017.

[15] L. Fei, G. Lu, W. Jia, J. Wen, and D. Zhang, "Complete binary representation for 3-D palmprint recognition," *IEEE Trans. Instrum. Meas.*, vol. 67, no. 12, pp. 2761–2771, Dec. 2018.

[16] L. Fei, B. Zhang, W. Jia, J. Wen, and D. Zhang, "Feature extraction for 3-D palmprint recognition: A survey," *IEEE Trans. Instrum. Meas.*, vol. 69, no. 3, pp. 645–656, Mar. 2020.

[17] J.-G. Wang, W.-Y. Yau, A. Suwandy, and E. Sung, "Person recognition by fusing palmprint and palm vein images based on 'Laplacianpalm' representation," *Pattern Recognit.*, vol. 41, no. 5, pp. 1514–1527, 2008.

[18] P. Chen, B. Ding, H. Wang, R. Liang, Y. Zhang, W. Zhu, and Y. Liu, "Design of low-cost personal identification system that uses combined palm vein and palmprint biometric features," *IEEE Access*, vol. 7, pp. 15922–15931, 2019.

[19] S. Cho, B.-S. Oh, K.-A. Toh, and Z. Lin, "Extraction and cross-matching of palm-vein and palmprint from the RGB and the NIR spectrums for identity verification," *IEEE Access*, vol. 8, pp. 4005–4021, 2020.

[20] W. Y. Choi and K. K. Park, "Fingerprint imaging of dry finger using photoacoustics," *J. Acoust. Soc. Amer.*, vol. 141, no. 3, pp. EL205–EL209, Mar. 2017.

[21] Y. Wang, Z. Li, T. Vu, N. Nyayapathi, K. W. Oh, W. Xu, and J. Xia, "A robust and secure palm vessel biometric sensing system based on photoacoustics," *IEEE Sensors J.*, vol. 18, no. 14, pp. 5993–6000, Jul. 2018.

[22] A. Iula, "Ultrasound systems for biometric recognition," *Sensors*, vol. 19, no. 10, p. 2317, May 2019.

[23] H. Park and Y. Roh, "Design of ultrasonic fingerprint sensor made of 1–3 piezocomposites by finite element method," *Jpn. J. Appl. Phys.*, vol. 56, no. 7S1, Jul. 2017, Art. no. 07JD06.

[24] A. Savoia, G. Caliano, A. Iulat, C. Longo, A. Caronti, R. Carotenuto, and M. Pappalardo, "Design and fabrication of a cMUT probe for ultrasound imaging of fingerprints," in *Proc. IEEE Int. Ultrason. Symp.*, Oct. 2010, pp. 1877–1880.

[25] N. Lamberti, G. Caliano, A. Iula, and A. S. Savoia, "A high frequency cMUT probe for ultrasound imaging of fingerprints," *Sens. Actuators A, Phys.*, vol. 172, no. 2, pp. 561–569, Dec. 2011.

[26] W. Y. Choi, Y. S. Kwak, and K. K. Park, "Fingerprint imaging system based on capacitive micromachined ultrasonic transducer by using impediography method including direct touch and waveguide methods," *IEEE Trans. Ultrason., Ferroelectr., Freq. Control*, vol. 66, no. 2, pp. 402–411, Feb. 2019.

[27] Y.-Q. Chen, Y.-X. Li, Y. Chen, Z.-Y. Ju, L.-Q. Tao, Y. Pang, Y. Yang, and T.-L. Ren, "Large-scale and high-density pMUT array based on isolated sol-gel PZT membranes for fingerprint imaging," *J. Electrochem. Soc.*, vol. 164, no. 7, pp. B377–B381, 2017.

[28] C. Peng, M. Chen, H. Wang, J. Shen, and X. Jiang, "P(VDF-TrFE) thin-film-based transducer for under-display ultrasonic fingerprint sensing applications," *IEEE Sensors J.*, vol. 20, no. 19, pp. 11221–11228, Oct. 2020.

[29] H.-Y. Tang, Y. Lu, X. Jiang, E. J. Ng, J. M. Tsai, D. A. Horsley, and B. E. Boser, "3-D ultrasonic fingerprint sensor-on-a-chip," *IEEE J. Solid-State Circuits*, vol. 51, no. 11, pp. 2522–2533, Nov. 2016.

[30] X. Jiang, H.-Y. Tang, Y. Lu, E. J. Ng, J. M. Tsai, B. E. Boser, and D. A. Horsley, "Ultrasonic fingerprint sensor with transmit beamforming based on a PMUT array bonded to CMOS circuitry," *IEEE Trans. Ultrason., Ferroelectr., Freq. Control*, vol. 64, no. 9, pp. 1401–1408, Sep. 2017.

[31] Qualcomm Technologies. (2019). Accessed: Mar. 13, 2019. [Online]. Available: https://www.qualcomm.com/solutions/mobile-computing/features/fingerprint-sensors

[32] A. Iula, G. E. Hine, A. Ramalli, F. Guidi, E. Boni, A. S. Savoia, and G. Caliano, "An enhanced ultrasound technique for 3D palmprint recognition," in *Proc. IEEE Int. Ultrason. Symp. (IUS)*, Jul. 2013, pp. 978–981.

[33] A. Iula, A. S. Savoia, and G. Caliano, "An ultrasound technique for 3D palmprint extraction," *Sens. Actuators A, Phys.*, vol. 212, pp. 18–24, Jun. 2014.

[34] A. Iula and D. Nardiello, "Three-dimensional ultrasound palmprint recognition using curvature methods," *J. Electron. Imag.*, vol. 25, no. 3, Jun. 2016, Art. no. 033009.

[35] A. Iula and D. Nardiello, "3-D ultrasound palmprint recognition system based on principal lines extracted at several under skin depths," *IEEE Trans. Instrum. Meas.*, vol. 68, no. 12, pp. 4653–4662, Dec. 2019.

[36] D. Nardiello, M. Calia, and A. Iula, "An enhanced ultrasound technique for 3D palmprint recognition," in *Proc. IEEE Int. Ultrason. Symp. (IUS)*, Sep. 2016, Art. no. 7728839.

[37] D. Nardiello and A. Iula, "A new recognition procedure for palmprint features extraction from ultrasound images," in *Applications in Electronics Pervading Industry, Environment and Society* (Lecture Notes in Electrical Engineering), vol. 512. Berlin, Germany: Springer-Verlag, 2019, pp. 113–118.

[38] A. Iula and M. Micucci, "Palmprint recognition based on ultrasound imaging," in *Proc. 42nd Int. Conf. Telecommun. Signal Process. (TSP)*, Jul. 2019, pp. 621–624.

[39] A. Iula and M. Micucci, "Experimental validation of a reliable palmprint recognition system based on 2D ultrasound images," *Electronics*, vol. 8, no. 12, p. 1393, Nov. 2019.

[40] A. Iula and M. Micucci, "Palmprint recognition through a reliable ultrasound acquisition system and a 3D template," in *Sensors and Microsystems* (Lecture Notes in Electrical Engineering), vol. 629. Cham, Switzerland: Springer, 2020, pp. 207–213.

[41] A. Fenster, S. Tong, H. N. Cardinal, C. Blake, and D. B. Downey, "Three-dimensional ultrasound imaging system for prostate cancer diagnosis and treatment," *IEEE Trans. Instrum. Meas.*, vol. 47, no. 6, pp. 1439–1447, Dec. 1998.

[42] A. Fenster, G. Parraga, and J. Bax, "Three-dimensional ultrasound scanning," *Interface Focus*, vol. 1, no. 4, pp. 503–519, Aug. 2011.

[43] M. R. Morgan, J. S. Broder, J. J. Dahl, and C. D. Herickhoff, "Versatile low-cost volumetric 3-D ultrasound platform for existing clinical 2-D systems," *IEEE Trans. Med. Imag.*, vol. 37, no. 10, pp. 2248–2256, Oct. 2018.

[44] J. D. Ruijter, M. van Sambeek, F. van de Vosse, and R. Lopata, "Automated 3D geometry segmentation of the healthy and diseased carotid artery in free-hand, probe tracked ultrasound images," *Med. Phys.*, vol. 47, no. 3, pp. 1034–1047, Mar. 2020.

[45] A. Iula, D. Nardiello, A. Ramalli, and F. Guidi, "3D ultrasound palmprint recognition system based on a mechanically tilted linear probe," in *Proc. IEEE Int. Ultrason. Symp. (IUS)*, Oct. 2015, pp. 1–4.

[46] P. Tortoli, L. Bassi, E. Boni, A. Dallai, F. Guidi, and S. Ricci, "ULA-OP: An advanced open platform for ultrasound research," *IEEE Trans. Ultrason., Ferroelectr., Freq. Control*, vol. 56, no. 10, pp. 2207–2216, Oct. 2009.

[47] W. Burger and M. J. Burge, *Principles of Digital Image Processing*. London, U.K.: Springer, 2009.

[48] R. C. Gonzalez and R. E. Woods, *Digital Image Processing*, 3rd ed. Upper Saddle River, NJ, USA: Prentice-Hall, 2006.

[49] M.-K. Kim, "Palmprint recognition based on line and slope orientation features," *J. Inf. Sci. Eng.*, vol. 27, pp. 1219–1232, Jul. 2011.

[50] L. Fei, G. Lu, W. Jia, S. Teng, and D. Zhang, "Feature extraction methods for palmprint recognition: A survey and evaluation," *IEEE Trans. Syst., Man, Cybern. Syst.*, vol. 49, no. 2, pp. 346–363, Feb. 2019.

[51] A. Garg and V. Khandelwal, "Speckle noise reduction in medical ultrasound images using modelling of shearlet coefficients as a Nakagami prior," *Adv. Electr. Electron. Eng.*, vol. 16, no. 4, pp. 538–549, Dec. 2018.
[52] J.-S. Lee, "Digital image enhancement and noise filtering by use of local statistics," *IEEE Trans. Pattern Anal. Mach. Intell.*, vol. PAMI-2, no. 2, pp. 165–168, Mar. 1980.
[53] D. T. Kuan, A. A. Sawchuk, T. C. Strand, and P. Chavel, "Adaptive noise smoothing filter for images with signal-dependent noise," *IEEE Trans. Pattern Anal. Mach. Intell.*, vol. PAMI-7, no. 2, pp. 165–177, Mar. 1985.
[54] S. Aja-Fernandez and C. Alberola-Lopez, "On the estimation of the coefficient of variation for anisotropic diffusion speckle filtering," *IEEE Trans. Image Process.*, vol. 15, no. 9, pp. 2694–2701, Sep. 2006.
[55] A. Garg and V. Khandelwal, "Combination of spatial domain filters for speckle noise reduction in ultrasound medical images," *Adv. Electr. Electron. Eng.*, vol. 15, no. 5, pp. 857–865, Jan. 2018.
[56] V. S. Frost, J. A. Stiles, K. S. Shanmugan, and J. C. Holtzman, "A model for radar images and its application to adaptive digital filtering of multiplicative noise," *IEEE Trans. Pattern Anal. Mach. Intell.*, vol. PAMI-4, no. 2, pp. 157–166, Mar. 1982.
[57] S. Banerjee, S. S. Chaudhuri, R. Mehra, and A. Misra, "A comprehensive survey on frost filter and its proposed variants," in *Proc. 5th Int. Conf. Commun. Electron. Syst. (ICCES)*, Jun. 2020, pp. 109–114.
[58] Y. Yu and S. T. Acton, "Speckle reducing anisotropic diffusion," *IEEE Trans. Image Process.*, vol. 11, no. 11, pp. 1260–1270, Nov. 2002.
[59] H. Choi and J. Jeong, "Speckle noise reduction for ultrasound images by using speckle reducing anisotropic diffusion and Bayes threshold," *J. X-Ray Sci. Technol.*, vol. 27, no. 5, pp. 885–898, Oct. 2019.
[60] W. Wang, W. Wang, and Z. Hu, "Segmenting retinal vessels with revised top-bottom-hat transformation and flattening of minimum circumscribed ellipse," *Med. Biol. Eng. Comput.*, vol. 57, no. 7, pp. 1481–1496, Jul. 2019.
[61] A. Halder and S. Ghose, "Blood vessel extraction from retinal images using modified Gaussian filter and bottom-hat transformation," in *Computational Intelligence in Pattern Recognition* (Advances in Intelligent Systems and Computing), vol. 999. New York, NY, USA: Springer, 2020, pp. 357–363.
[62] X. Wu, K. Wang, and D. Zhang, "Palmprint texture analysis using derivative of Gaussian filters," in *Proc. Int. Conf. Comput. Intell. Secur.*, vol. 1, Nov. 2006, pp. 751–754.
[63] D. Tamrakar and P. Khanna, "Kernel discriminant analysis of block-wise Gaussian derivative phase pattern histogram for palmprint recognition," *J. Vis. Commun. Image Represent.*, vol. 40, pp. 432–448, Oct. 2016.
[64] A. Bruno, P. Carminetti, V. Gentile, M. L. Cascia, and E. Mancino, "Palmprint principal lines extraction," in *Proc. IEEE Workshop Biometric Meas. Syst. Secur. Med. Appl. (BIOMS)*, Oct. 2014, pp. 50–56.
[65] A. Iula and M. D. Santis, "Experimental evaluation of an ultrasound technique for the biometric recognition of human hand anatomic elements," *Ultrasonics*, vol. 51, no. 6, pp. 683–688, Aug. 2011.
[66] A. Iula, G. Hine, A. Ramalli, and F. Guidi, "An improved ultrasound system for biometric recognition based on hand geometry and palmprint," *Procedia Eng.*, vol. 87, pp. 1338–1341, 2014.
[67] A. Iula, "Biometric recognition through 3D ultrasound hand geometry," *Ultrasonics*, vol. 111, Mar. 2021, Art. no. 106326.
[68] M. De Santis, S. Agnelli, D. Nardiello, and A. Iula, "3D ultrasound palm vein recognition through the centroid method for biometric purposes," in *Proc. IEEE Int. Ultrason. Symp. (IUS)*, Sep. 2017, pp. 1–4.
[69] A. Iula, "Optimization and evaluation of a biometric recognition technique based on 3D ultrasound palm vein," in *Proc. IEEE Int. Ultrason. Symp. (IUS)*, Sep. 2020, pp. 1–4.
[70] J. Chen, Y. Wu, Y. Yang, S. Wen, K. Shi, A. Bermak, and T. Huang, "An efficient memristor-based circuit implementation of squeeze- and-excitation fully convolutional neural networks," *IEEE Trans. Neural Netw. Learn. Syst.*, to be published, doi: 10.1109/TNNLS.2020.3044047.
[71] H. Ran, S. Wen, Q. Li, Y. Yang, K. Shi, Y. Feng, P. Zhou, and T. Huang, "Memristor-based edge computing of blaze block for image recognition," *IEEE Trans. Neural Netw. Learn. Syst.*, early access, Dec. 29, 2020, doi: 10.1109/TNNLS.2020.3045029.
[72] J. Xiao, Z. Zeng, A. Wu, and S. Wen, "Fixed-time synchronization of delayed Cohen–Grossberg neural networks based on a novel sliding mode," *Neural Netw.*, vol. 128, pp. 1–12, Aug. 2020.
[73] W.-J. Niu, Z.-K. Feng, B.-F. Feng, Y.-S. Xu, and Y.-W. Min, "Parallel computing and swarm intelligence based artificial intelligence model for multi-step-ahead hydrological time series prediction," *Sustain. Cities Soc.*, vol. 66, Mar. 2021, Art. no. 102686.
[74] Butterfly Network. (2020). Accessed: Jun. 25, 2020. [Online]. Available: https://www.https://www.butterflynetwork.com/
[75] G. Caliano, R. Carotenuto, E. Cianci, V. Foglietti, A. Caronti, A. Iula, and M. Pappalardo, "Design, fabrication and characterization of a capacitive micromachined ultrasonic probe for medical imaging," *IEEE Trans. Ultrason., Ferroelectr., Freq. Control*, vol. 52, no. 12, pp. 2259–2269, Dec. 2005.
[76] B. A. Greenlay and R. J. Zemp, "Fabrication of linear array and top-orthogonal-to-bottom electrode CMUT arrays with a sacrificial release process," *IEEE Trans. Ultrason., Ferroelectr., Freq. Control*, vol. 64, no. 1, pp. 93–107, Jan. 2017.

ANTONIO IULA (Senior Member, IEEE) is currently an Associate Professor of Electronics with the University of Basilicata, Potenza, Italy. He has authored more than 120 papers in these fields published in international journals and conference proceedings. His research interests include piezoelectric transducer modeling and characterization for ultrasound applications in biomedical and industrial fields, and piezoelectric motors and actuators and ultrasound imaging for biometric applications. He has been involved in several national and international research programs.

MONICA MICUCCI is currently pursuing the M.S. degree in computer and information engineering with the University of Basilicata, Potenza, Italy. Her current research interests include ultrasound imaging and image processing.